# Nanoscale

## Accepted Manuscript

ROYAL SOCIETY OF CHEMISTRY

www.rsc.org/nanoscale

# Journal Name

## ARTICLE TYPE

# Optical antennas with multiple plasmonic nanoparticles for tip-enhanced Raman microscopy

Atsushi Taguchi,[a] Jun Yu,[a‡] Prabhat Verma[a] and Satoshi Kawata[*a]

Tip-enhanced Raman spectroscopy (TERS) has recently become one of the most important tools for analyzing advanced nano-devices and nano-materials, because it allows strong enhancement of weak Raman signal from the nanometric volume of a sample. However, consistent enhancement in TERS is still an issue and scientists have been struggling to fabricate good tips for reliable, strong and reproducible enhancement. There is a strong need to study the morphology and the arrangement of metal nanostructures near the tip apex for efficient plasmonic enhancement in TERS. Here, we present a study on the metal grains attached to the tip surface for producing higher and much consistent enhancement in TERS. Our study shows that the plasmonic enhancement strongly depends on the number of grains and on the their separations. We found through simulations that multiple grains arranged closely but discretely on a dielectric probe act as an efficient plasmonic antenna and that enhancement in TERS is maximum for an optimized number of grains. The number of grains and the nano-gap between them are crucial for reproducible enhancement. This promising result, which we also demonstrate and prove by experiments, will bring TERS to a new level, where it can be utilized with more confidence of large reproducible enhancement for those nano-sized samples that have extremely weak Raman scattering.

## 1 Introduction

Optical visualization of molecules with spatial resolution exceeding beyond Abbe's diffraction limit of light requires confinement of photons within an extremely tiny volume. The use of metallic nano tip to achieve such confinement was originally proposed more than 20 years ago[1,2], and hence became an indispensable technique in this decade to realize nano-resolution imaging of molecules. A metallic tip, usually made of noble metals such as Ag and Au, produces a strong optical field confined in the vicinity of the tip due to the excitation of plasmon resonances[3,4]. We have applied metallic probes for imaging molecular distribution through Raman scattering spectroscopy. Although Raman scattering of molecules is an extremely weak photon process, the metallic probe enhances the scattered signal by a factor of thousands to millions[5–8]. The tip scans the surface of the sample to obtain an image of molecular distribution in nanoscale[9–11]. This system has been called as the tip-enhanced Raman spectroscopy (TERS) microscope. The metallic structure of the probe is thus the key component for obtaining nano-resolution with large enhancement of the Raman scattering signal. The tip in TERS is usu-

ally controlled by the atomic force microscopy (AFM), scanning tunneling microscopy (STM) or shear force microscopy (SFM). A variety of probes with different metallic structures have been utilized and discussed in literatures including smoothly shaped and tapered metal wire for STM and SFM-based TERS[10,12], and metal film on Si[8,13], on SiO$_2$[14,15], or on AlF$_3$[14] cones for AFM-based TERS. However, the enhancements obtained from the tips in typical TERS experiments have not been consistently reproducible. Thus, there is a strong need to study the structure of the metal tip for efficient and reproducible enhancement.

In our experiments, we often use AFM-based TERS, where we fabricate the probes by thermal evaporation of silver on commercially available (raw or oxidized) silicon cantilever tips. Recently, along with the improvement of our skill in fabricating tips, we have noticed in the course of performing TERS that the Raman scattering drastically reduces when the tip is coated with smoother metallic layer. Motivated by this marked observation, here, we investigate the relationship between the surface morphology of the tip and the scattering efficiency of the TERS probe through numerical simulations and experimental verification. Unlike previous numerical studies dealing with a smooth conical tips[3,4], we investigate the role of metal grains on the plasmonic properties of a probe that is fabricated by thermal evaporation of metal. The plasmon resonance properties of a tip covered with granularly structured metal has not been discussed so far in litera-

[a] Osaka University, Department of Applied Physics, Suita, Osaka 565-0871, Japan. Fax: +81 (0)6 68797845; Tel: +81 (0)6 68797845; E-mail: kawata@ap.eng.osaka-u.ac.jp

‡ Present address: Nanophoton Corporation, Photonics Center, Suita, Osaka 565-0871, Japan.

tures, despite the insistent hypothesis that the metal grains within a metallized probe are important to obtain better enhancement in TERS [16]. Indeed, apart from the grain size and inter-granule separations, the number of metal grains at and near the tip apex drastically influence the plasmon resonance properties of the tip. The arrangement of metal grains with nanometric separation is analogous to plasmonic nanoparticle chains, studied by some researchers in the past. Maier et al. studied the coupled plasmon modes in nanoparticle chain waveguides [17,18], and discussed how plasmon resonance depends on both the number of particles and their separations. Kawata et al. discussed propagation of near-field light through stacked silver nanorods and showed remarkable broadening in plasmon resonance, which could be applied to multicolor image transfer with a sub-wavelength spatial resolution [19]. Jonathan et al. demonstrated a variety of plasmon modes including magnetic and Fano-like resonances using assembled clusters of plasmonic spheres [20]. Self-similar chain of metal particles for adiabatic plasmon nanofocusing was also demonstrated [21,22]. Similar to these studies, one would expect strong influence of grain arrangement near the tip apex on plasmon resonance in terms of resonance wavelength, broadening as well as enhancement. Our primary findings indicate that Raman enhancement maximizes for an optimal number of grains on a plasmonic tip and that the nano-gaps between these grains play a very important role in tuning plasmon resonance as well as in increasing the enhancement. To the best of our knowledge, this is the first report that examines the enhancement and the spectral properties of plasmons at the end of the tip for the number of grains as well as their arrangement. Finally, in order to verify our hypothesis, we experimentally demonstrate the effectiveness of the multiple-grain structure in TERS by imaging carbon nanotubes and graphene.

## 2 Results and discussion

Figure 1(a) shows a model of tip-sample-substrate configuration used in our simulations. We assume that the TERS probe is $1\,\mu m$ long and is made of a $SiO_2$ conical tip coated with Ag [15]. The diameter and the cone angle of the $SiO_2$ tip are 10 nm and 40 degrees, respectively. A molecule (marked by a red dot in Fig. 1(a)), acting as a scattering dipole, is located on a $SiO_2$ substrate right beneath the tip. The distance between tip and substrate is 4 nm. A radially polarized light is focused and incident on the upper surface of the substrate from the bottom to excite the molecule through an objective lens of NA 1.4. The tightly focused radially polarized light produces a field polarized parallel to the tip axis at its focus, which facilitates the excitation of a longitudinal mode of plasmon along the tip axis [23]. The incident light covers a broad spectral range between 300 and 800 nm. At the silver tip, the localized mode of surface plasmon is excited, which produces strong Rayleigh scattering around the plasmon resonance that can be detected in the far-field. In addition, the localized near-field photons produced by the resonant excitation of the localized plasmons excite molecular vibrations in the sample to produce Raman scattering. The Raman scattering signal is converted back to far-field by the tip apex and is detected in the far-field through the same optics used for the excitation.
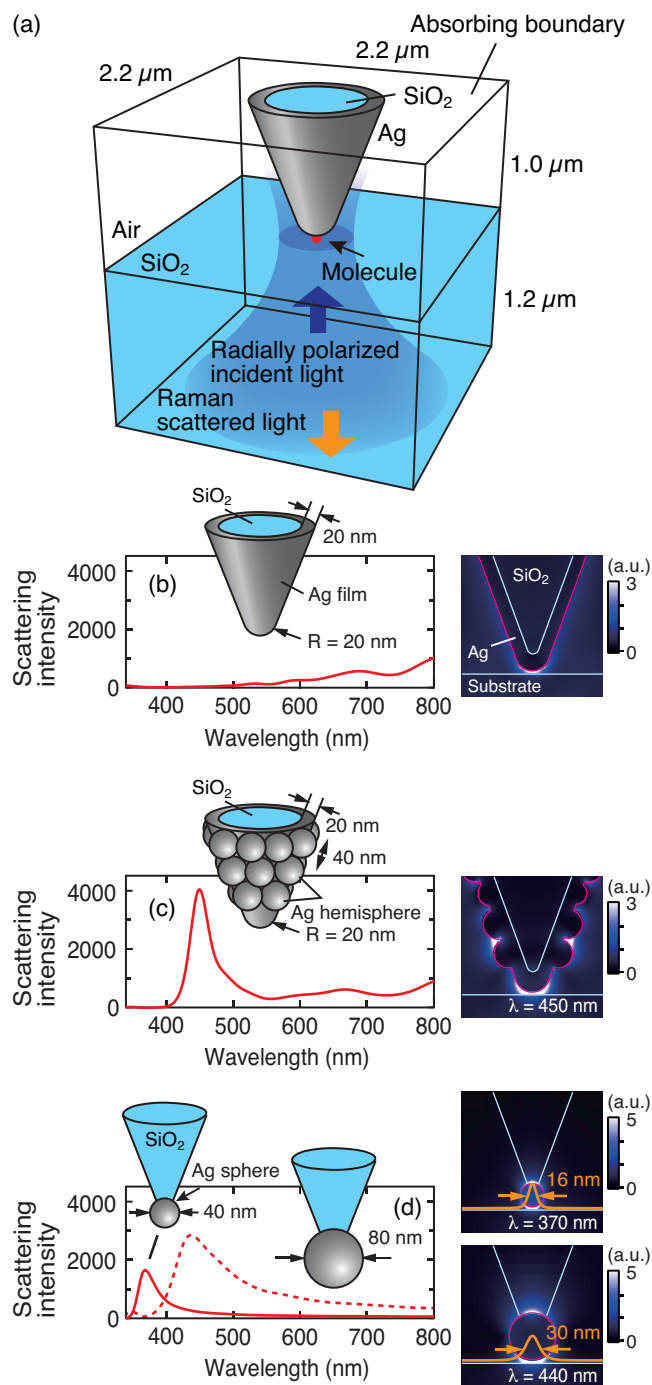


**Fig. 1** Scattering spectra of a molecule near a tip with various Ag structures normalized to that without a tip. (a) Model of TERS system used in simulations. (b) Smooth Ag film on $SiO_2$ cone. (c) Rough corrugated Ag film on $SiO_2$ cone. (d) Single Ag particle with a diameter of 40 nm (solid line) and 80 nm (dashed line) attached on $SiO_2$ cone. The cross-sectional distributions of the excited field are shown in the right panels at the wavelength of 488 nm for (b) and at the corresponding resonance wavelengths for (c) and (d). The physical parameters of the tips are shown in the insets.

The left panels of Figs. 1(b)–(d) show the scattering spectra detected in the far-field for the tips with different metallic structures shown in the insets, normalized to that without probe. These spectra correspond to the Rayleigh scattering of the molecule at the tip apex. Figure 1(b) shows the scattering spectrum for a $SiO_2$ tip that is entirely covered with a smooth Ag film (or layer) with a thickness of 20 nm. No pronounced resonance peak is seen in the spectrum in the visible range, indicating that a smooth tip with infinitely long metal structure does not act as a plasmonic antenna in the visible range. Rather, the smooth probe behaves as a waveguide, on which the plasmon propagates non-radiatively[24–26], and eventually decays by metallic loss. While one cannot expect resonant field enhancement for a smooth tip, the field is still localized with some enhancement at the apex of a smooth probe, as seen in the cross-sectional distribution of the excited field shown in the right panel of Fig. 1(b), due to the lightning rod effect. Owing to the non-resonant nature, the enhancement is only weakly dependent on the wavelength, which can explain the reported reproducible enhancement in TERS using smooth gold pyramids[27]. The tips used in STM-based TERS are made of solid metal with smooth surface. However, researchers have reported good enhancement in STM-TERS. This is because the use of a metallic substrate is essential for controlling the tunneling current in STM. This creates a so-called gap-mode near the tip apex that confines the light in the tip-substrate gap. Therefore, even a very smooth tip in STM-TERS still shows enhancement, however, it is relatively wavelength independent and has less possibilities to either tune or improve plasmon resonance.

In contrast to a smooth tip, the spectrum shown in the left panel of Fig. 1(c) has a significantly pronounced peak at the wavelength of 450 nm. This spectrum is obtained for an Ag-coated probe that is corrugated with hemispherical Ag grains with a radius of 20 nm (see the inset). The corrugated Ag film entirely covers the 1 $\mu$m-long $SiO_2$ cone probe. This result demonstrates that grains are necessary for obtaining resonance. We have compared the scattering intensity of the peak at 450 nm in Fig. 1(c) with and without a tip, and estimated an enhancement factor of about 4,000 in intensity. The mechanism of enhancement by the grains can be explained by optical antenna theory[28–30]. Grains work as resonant dipole antennas which receive/transmit optical radiation between the far-field and near-field. Its size predominantly determines the resonance wavelength of the optical antenna. While the size of radio wave or microwave antenna is a multiple integer of half wavelength of the signal, the length of an optical antenna is much shorter than the wavelength of light because the wavelength of plasmon polaritons excited in the visible is much shorter than that of light propagating in free space[31].

Interestingly, our simulated spectrum in Fig. 3(c) shows a similar spectral response that was experimentally observed in the past for an Ag corrugated film deposited on a $SiO_2$ cone[15]. The overall consistency between the simulation and experiment further corroborates the necessity of grains for obtaining a resonance in the visible region.

A single particle also works as an antenna. For example, Fischer and Pohl used a single nanoparticle on a flat metal film for plasmonic nano-imaging[32], and Sugiura et al. used an isolated

metal particle as probe of a near-field fluorescence microscope in solution[33]. On the other hand, Okamoto et al.[34] and Kalkbrenner et al.[35] used a gold nanoparticle mounted on the end of an AFM probe and glass fiber probe, respectively, for near-field scanning optical microscopy. Barsegova et al. demonstrated a fabrication of metal nanoparticles at the tip of glass fiber probe with size-controllable manner[36]. Umakoshi et al. grew an Ag nanoparticle directly on the tip apex by photoreduction and showed higher TERS enhancement compared to regular tips[37]. Ando et al. applied single nanoparticle near-field Raman microscope for observing cellular molecules inside a living cell[38]. All these reports indicate that a single particle can be used to resonantly enhance the light near the antenna. In our study, we also found similar results, but interestingly, we also found that single particle does not provide the best enhancement. In the left panel of Fig. 1(d), we show the scattering spectrum for a single Ag particle with a diameter of 40 nm (solid line) and 80 nm (dashed line) attached on a $SiO_2$ cone (inset). The resonance peak for the 40 nm particle, which has the same size as the particles in Fig. 1(c), appears at 370 nm, considerably blue-shifted compared with that for the probe with rough corrugated film (Fig. 1(c)). Since the probe shows almost no enhancement in the visible range, a single Ag sphere with the size of 40 nm is not an efficient probe of TERS with visible excitation. On the other hand, a spherical particle with 80 nm diameter shows a stronger enhancement centered around 440 nm in the visible range. The resonance peak around 440 nm has also been observed experimentally in the past for a similar size of Ag particle (diameter of ∼100 nm) fabricated at the apex of a $SiO_2$ tip[39]. This enhancement is weaker than that seen in Fig. 1(c) and the confinement of light (or spatial resolution) is destroyed due to the larger size of the particle, as shown by the cross-sectional line profiles of the field intensities between the tips and substrates in the right panel of Fig. 1(d).

Next, we changed the number of grains (metallic nanoparticles) on the probe to examine the possible variation in enhancement. As illustrated in Fig. 2(a), the grains are arranged in a certain way on the surface of $SiO_2$ cone. The diameters of Ag particles are 40 nm, and the cone angle of the $SiO_2$ probe is 40 degrees. The particles are not connected to each other but are separated with a gap of 4 nm. Figure 2(b) shows the scattering spectra of a molecule obtained with tips having different number of Ag particles. The spectrum for the single particle probe ($N = 1$, top panel) is the same as the one already shown in Fig. 1(d). When the particle number was increased to $N = 4$ (middle panel), the scattering intensity became significantly stronger and the resonance was shifted to 430 nm. At the resonance, the scattering intensity for the four-particle probe is about eight times stronger than that for a single-particle probe. The reason for the increase in scattering intensity with the increase in the number of particles is that the aggregation of particles works as an efficient coupler that couples in the incident light from the far-field and couples out the scattered light to the far-field, while the particle closest to the sample molecule works as the near-field antenna to excite the sample molecule. When the number of particles are further increased to $N = 9$ (bottom panel), the scattering intensity is decreased and the resonance is further shifted to 440 nm. The de-
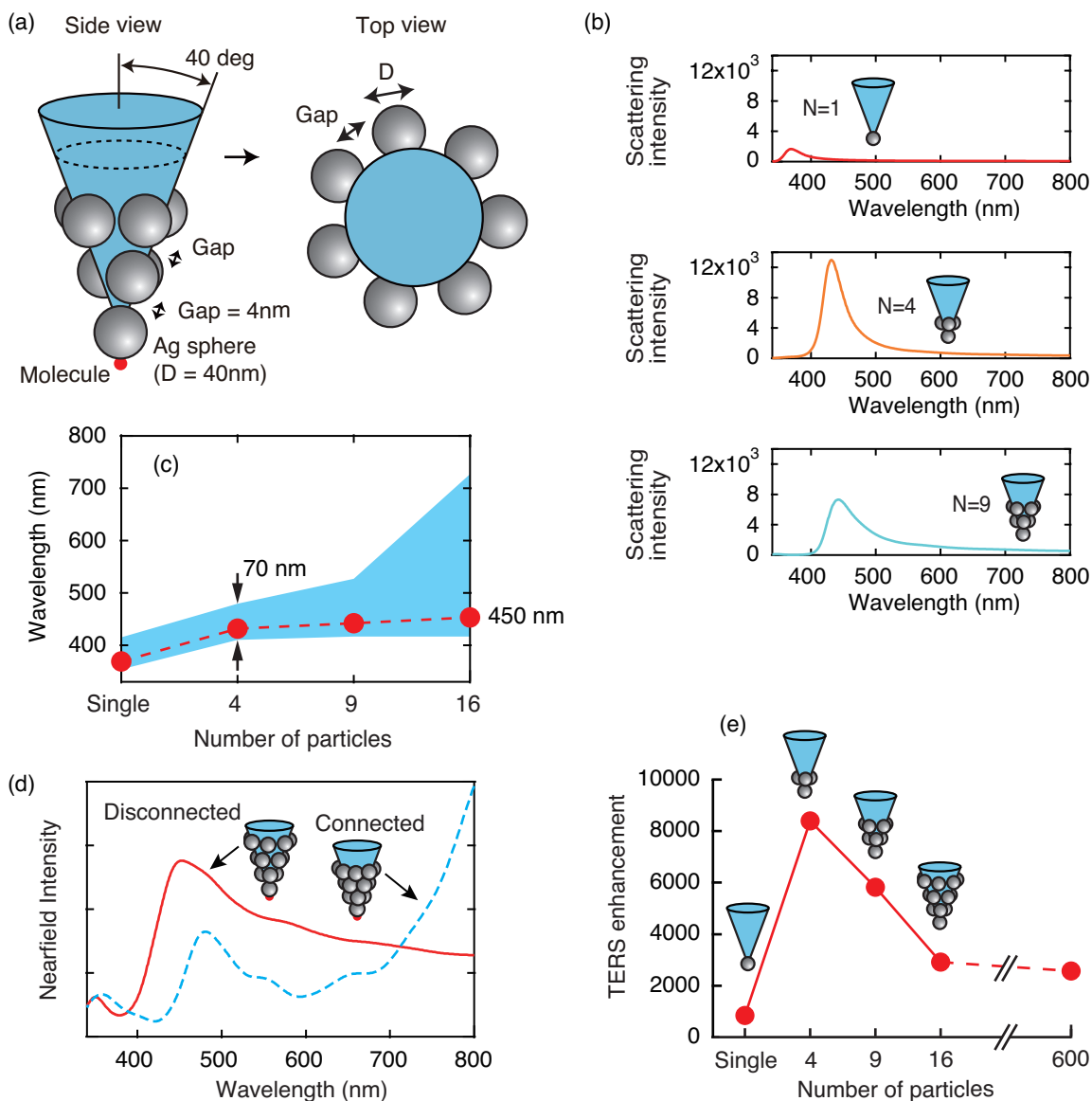
**Fig. 2** TERS enhancement of multiple grain probe. (a) Arrangement of multiple grains on $SiO_2$ cone. (b) Scattering spectra of a molecule near the tip of the probe having one (top), four (middle) and nine (bottom) particles, normalized to that without the probe. (c) The peak wavelength (red circle) and half-maximum width (blue region width) of plasmon resonance are shown as a function of the number of particles. (d) Near-field intensity spectrum at the tip of disconnected (solid line) and connected (dashed line) 16-particle probe, normalized to that without tip. (e) TERS enhancement is plotted as a function of the number of particles.

crease of the scattering for the large number of particles can be explained by the propagation loss of the plasmons through particle chain over a long distance[17].

It is also interesting to note how the peak shifts and spreads as the number of grains increases. Figure 2(c) summarizes how the plasmon resonance peak shifts and broadens as the numbers of grains increases. As one can see, the peak shifts towards longer wavelength with increasing number of particles, and asymptotically approaches to ∼450 nm. This behavior of peak shift is somewhat similar to the one observed in the experiment of plasmon propagation through a nanoparticle chain[17], where the authors launched plasmons at the particle at one end, which propagates through the adjacent particles successively via resonant coupling. However, in our case, all particles are collectively excited and thus we have the case of resonance in a multiple grain antenna. At the same time, the resonance peak width (shown as the blue belt) broadens as the number of grains increases. In the case of the four-particle probe, the peak width is 70 nm (corresponding to 3,300 cm$^{-1}$), which is broad enough to cover the entire vibrational fingerprint for Raman scattering of most of the samples of interest. Since Raman spectroscopy is intrinsically a multi-color technique, such a broadband enhancement is beneficial for TERS spectroscopy.

In an earlier report, broadening of resonance spectrum was predicted in stacked silver nanorods[19]. Notably, the broadening was seen only when there was a nano-gap between the adjacent nanorods. If the gap was removed, the chain behaved like a long rod and thus multiple peaks appeared rather than a broadband. This indicates that the existence or absence of gap between grains is an important issue that needs to be examined. Figure 2(d) shows scattering spectra simulated in the near-field for a probe with 16 particles. When the grains are disconnected, a broad resonance peak is seen at 450 nm (solid line). If the grains are connected, the spectrum shows weaker enhancement with multiple modes in the visible region (dashed line). The peak seen at 480 nm in connected grains represents the second-order resonance, while the fundamental dipolar resonance mode appears in the infrared, outside the spectral range shown in Fig. 2(d). We do not consider the fundamental mode in this study since Raman scattering becomes considerably inefficient in the infrared region due to the forth power dependence of Raman scattering cross-section on optical frequency. This shows a clear indication that probes with disconnected metallic particles are much better than the probes with connected particles for TERS in the visible region.

Finally, we evaluated how TERS enhancement depends on the number of grains. We assume that the wavelength of Raman excitation is set at the peak wavelength of the plasmon resonance for each probe. In the reported literatures, it is common to evaluate TERS enhancement simply as the fourth power of the field enhancement at the tip apex[40,41], neglecting the wavelength shift from the excitation. In our evaluation, we also take into account the Raman shift. This is done by spectrally averaging the scattering intensity over the spectral range between 0 cm$^{-1}$ and 3000 cm$^{-1}$. The obtained value, which represents an expected enhancement factor for Raman scattering, is multiplied by the enhancement factor at Raman excitation wavelength to obtain a value of TERS enhancement. The result is shown in Fig. 2(e) as a function of the number of grains. From this graph, we found that the probe with four particles shows the highest value of enhancement, as was also seen for Rayleigh scattering in Fig. 2(b). The enhancement factor of the four-particle probe is about 8,400, almost 10 times higher than that of a single particle probe. In fact, the optimal number of grains showing the highest enhancement depends upon the other tip parameters (such as particle shape, size, and inter-particle distance), which we will discus later in more details. In a real experiment, the typical number of grains for a 1-$\mu$m-long conical probe is ∼600, which is also shown in Fig. 2(e). This 600-grain probe enhances Raman scattering by factor of 2,900, three times higher than that of a single-particle probe.

In order to obtain further insight into the mechanism of tip-enhancement produced by multiple grains, we considered a simple arrangement of the grains where the metal particles are aligned in a linear chain on the tip surface. We calculated the field intensity enhancement at the tip by changing the particle shape, size, and gap distance, and investigated how the enhancement depends on these parameters. In our simulations, the chain was illuminated by a plane wave normally incident on the chain body with a polarization along the chain axis. Figure 3(a) shows the calculated field intensity enhancement at the end of the particle chain (marked as the red dot in the left panel) for different number of particles. The diameter and the gap length are 40 nm and 4 nm, respectively, which are the same as in Fig. 2. For the single particle, the plasmon resonance is observed at 370 nm. The resonance peak shifts when another particle is added. The resonance of longitudinally coupled modes shifts to longer wavelength as the number of particles increases, which is similar to what we had observed for multiple grain probe in Fig. 2. The enhancement also changes with the number of particles. The enhancement for two particles (or dimer) is stronger than that for single particle. While researchers have extensively studied Raman enhancement at the gap or junctions of particle dimer[40,42–44], our calculations demonstrated that the enhancement becomes stronger not only at the gap but also at one end of the dimer. The strongest enhancement in Fig. 3(a) is observed for three particles. This optimal number of particles changes when gap distance is changed. Figure 3(b) shows the simulation results for the same situation as in Fig. 3(a), except that the gap size was reduced from 4 nm to 1 nm. The optimal number of particles for maximum enhancement changes to $N = 4$ for reduced gap size. The observed difference of the optimal number is due to the fact that, for smaller gap, the field is strongly concentrated inside the gap rather than on the metal surface, which reduces the propagation loss of surface plasmon and allows plasmon propagation for longer chain. Also, the field intensity enhancements for any number of particles become considerably stronger compared with the case of 4 nm gap. While the enhancement becomes higher for the smaller gap, the amount of peak shifts also become larger. This means TERS enhancement becomes more sensitive to the number of particles for a given Raman excitation wavelength. While the smaller gap distance promotes stronger interaction between the adjacent particles, the stronger interaction can also be induced by changing the shape
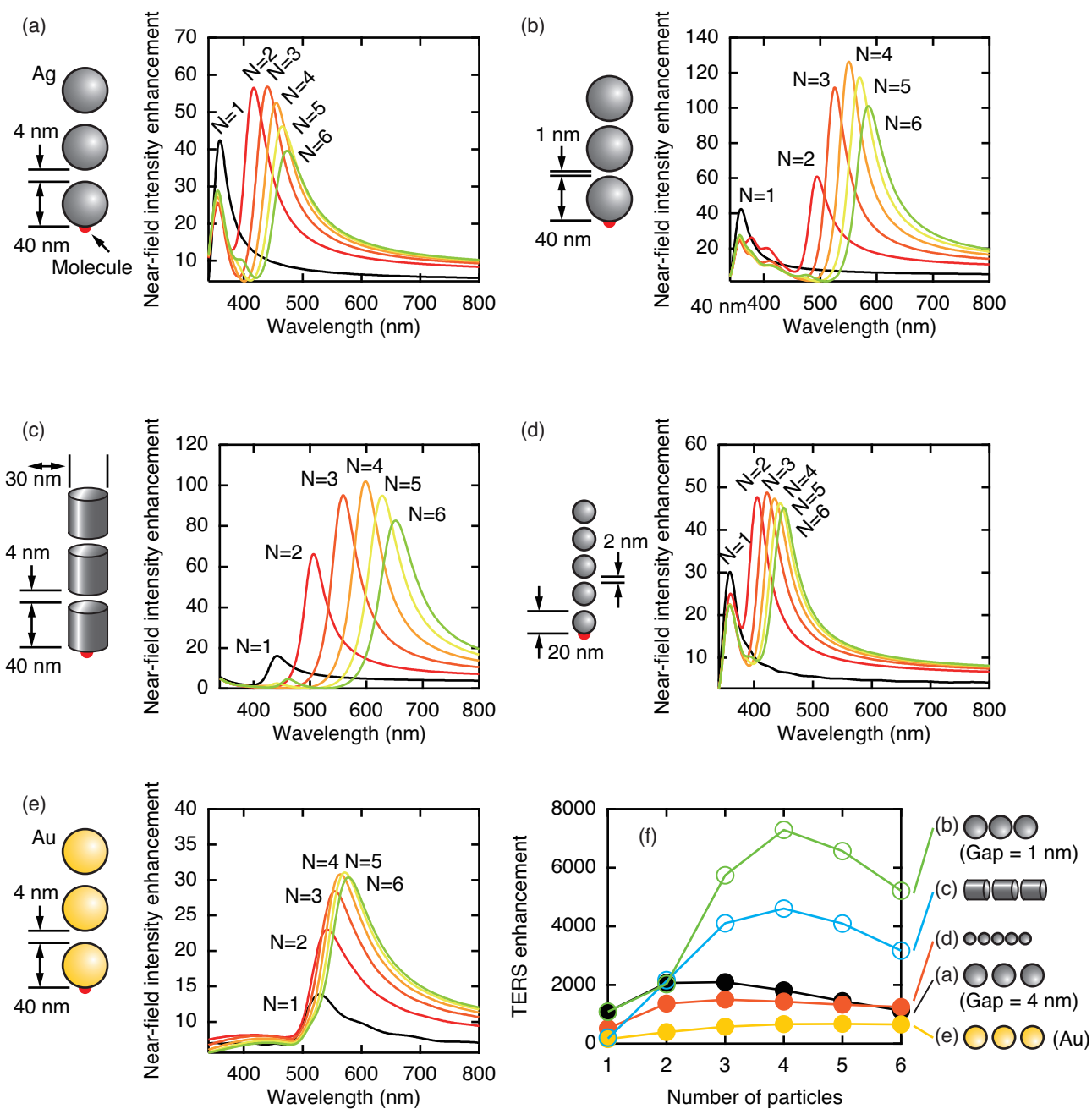
**Fig. 3** Field intensity enhancement at the end of linear particle chains. (a)–(d) Ag particles with different particle shape, size, and gap distance are aligned linearly. (e) Au particles are aligned linearly. (f) TERS enhancements are shown for different particle shape, size, and gap distance as a function of the number of particles.

of particles, for example, from sphere to rod. Figure 3(c) shows the result for a chain consisting of rods with a length, diameter, and gap distance of 40, 30 and 4 nm, respectively. In comparison of the spherical particles, the rod-like particles change the geometry at gap where larger surface areas of the adjacent particles face each other at the gap and hence result in stronger plasmon coupling at the gap. The optimal number of particles for the strongest enhancement for the rod-shaped particles is again four, although the gap distance is large. This result demonstrates that the strength of the longitudinal coupling between the adjacent particles significantly affects the spectral behavior of the multiple particle antenna. The strong inter-particle coupling for rods manifest itself also as the large amount of peak shifts compared to the case of spherical particles having the same gap distance of 4 nm (Fig. 3(a)). As already discussed, the metallic loss is the main cause for the decrease of enhancement beyond the optimal number of particles. To reduce the metallic loss, it is beneficial to reduce the surface area of metal. We thus examined smaller particles with diameters of 20 nm and a gap distance of 2 nm, as shown in Fig. 3(d). Similar to the larger particle chain, here we chose the gap to be one-tenth of the particle size. Here, we find that the results are comparable with those obtained in the case of 40 nm particles (Fig. 3(a)), expect that the total enhancements are reduced, which is expected for smaller particles. However, comparing the enhancement of two 20 nm-particles with that of one-40 nm particle, we observed stronger enhancement for two 20 nm-particles, even though the net antenna lengths are almost identical in the two cases. It is also interesting to examine a chain made of gold spheres, which is shown in Fig. 3(e). For the same parameters as in Fig. 3(a), the enhancement in Fig. 3(e) is maximum for five particles. The peak shift in gold is relatively small but the peak width broadens significantly with increasing number of particles. The behavior is similar to the case of silver particles, the total enhancement is weaker than silver case. Therefore, we concluded that silver particles are better for TERS in visible region. As a summary of the above discussion, in Fig. 3(f), we compared the TERS enhancement as the number of particles for different grain configurations examined above. As seen from the graph, the strongly coupled particles, such as rods or spherical particles with smaller gap, provide extremely high value of TERS enhancement, but the enhancement is also sensitively dependent on the number of particles. On the other hand, the maximum possible TERS enhancement for relatively weakly coupled particles is moderate, and the enhancement in this case is less sensitive to the number of particles.

Finally, we performed some experiments to verify the effectiveness of disconnected multiple grain probes for TERS imaging. To begin with, we show in Fig. 4(a) the Raman spectra of a graphene sample, which was measured by bringing a silver probe whose surface was corrugated with connected grains (left panel) close to the sample. The graphene sample used in the present experiment was uniformly thick with a large area of several tens of $\mu m^2$. Such a planar sample is ideal for evaluating the enhancement factor[45]. The scanning electron microscope (SEM) image of the probe used in the experiment is shown in the inset. The spectrum in red shows a Raman spectrum when the probe tip was near the

sample, while that in blue shows the same expect that the probe tip was far from the sample. As seen from the figure, Raman signal intensities at G-band (1590 cm$^{-1}$) and 2D-band (2700 cm$^{-1}$) were increased with the enhancement factors of about 880 and 1,100, respectively. The enhancement at G-band is weaker than that at 2D-band, which can be explained by the spectrally narrow resonance of the connected grain probe, as explained before for Fig. 2(d). For comparison, Fig. 4(a) also shows the result of the same experiment but with a probe that had smoother surface (right panel). It is seen from the SEM image that the surface corrugation on the surface of the probe has a period of several hundreds of nanometers, which is much larger than the wavelength of the surface plasmons, and hence, the probe can be categorized as a smooth tip. Both peaks at G- and 2D-bands are only weakly enhanced when the tip is near to the sample, which corresponds to an enhancement factor of only 230. The smaller enhancement factor observed for the smooth tip is consistent with the result of simulation shown in Fig. 1(b), where no resonance was observed for enhancement. From these results, we conclude that roughness on silver is crucial for obtaining enhancement as predicted from our simulations.

Next, we arranged silver grains discretely on SiO$_2$ cone. Figure 4(b) shows a SEM image of the probe used in this experiment. Judging from the SEM image, the grain at the probe end has a diameter of 40 nm. We fabricated the disconnected grains on SiO$_2$ cone by heating up the SiO$_2$ cone to a temperature of 600 K during the Ag deposition. We have fabricated 30 probes under the identical conditions. All of them had the same surface morphologies as judged from the average grain size and inter-grain separations near the apex in SEM observations. Figure 4(c) shows the Raman spectra of the same graphene sample used in Fig. 4(a), obtained with the probe shown in Fig. 4(b). The Raman intensities of G- and 2D-bands were found to be increased by about 25 times when the probe was near the graphene than when it was far, which corresponds to an enhancement factor of 5,500. The enhancement factor was calculated as the ratio of the detected near-field Raman intensity per unit sample volume to the detected far-field Raman intensity per unit sample volume[16]. The detection volume for far-field comes from the size of diffraction-limited spot, while we assumed a 14 nm-diameter-spot for near-field detection, as demonstrated in the TERS image of carbon nanotube (CNT) shown in Fig. 5(b). The obtained value of Raman enhancement factor is considerably larger than the value obtained with a tip that had connected grains (Fig. 4(a)). Unlike the spectrum obtained with the connected grain probe (Fig. 4(a)), the peaks at G- and 2D-bands are nearly equally enhanced in the spectrum obtained with the disconnected grain probe, which is due to the broadened plasmon resonance as predicted in our simulation shown in Fig. 2(c). We have repeated experiments with many probes fabricated under the identical conditions, and observed similar Raman enhancement, which proves a satisfactory repeatability of the tip preparation method described above.

We further applied the disconnected grain probe for imaging CNT bundles. Figure 5(a) shows the Raman spectra of an isolated bundle of CNTs obtained with the probe. The probe used in the experiment is shown in the inset. The silver grains are sepa-
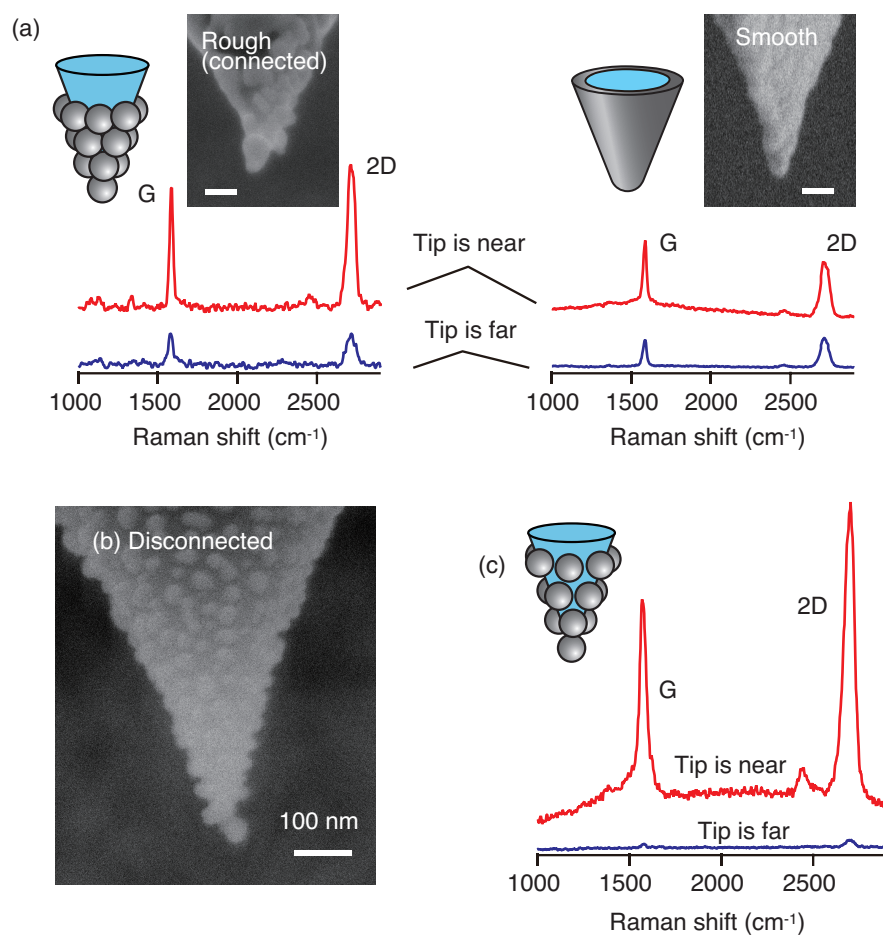
**Fig. 4** (a) Raman spectra of graphene sheets scattered with Ag tip having rough (left panel) and smooth (right panel) surface. The spectra are vertically shifted for clarity. The insets show scanning electron micrograph (SEM) of the tip used. The scale bar is 100 nm. (b) SEM of disconnected Ag grains coated on $SiO_2$ cone probe. (c) Raman spectra of a graphene sheet measured with the disconnected multiple grain tip. The spectra are vertically shifted for clarity.
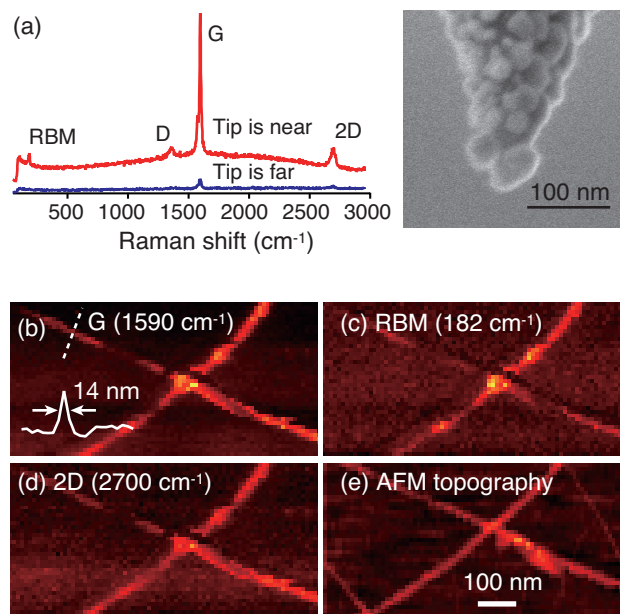
**Fig. 5** (a) Raman spectra of carbon nanotube (CNT) bundles scattered with the disconnected multiple grain tip. The spectra are vertically shifted for clarity. The SEM image of the probe having disconnected Ag grains is shown in the inset. (b)–(d) TERS images of CNTs measured with the disconnected multiple grain tip are shown at G-band, radial breathing mode (RBM), and 2D-band, respectively. The line profile of Raman intensity is shown in (b) along the dashed line. (e) Topographic image of CNT simultaneously taken during scan.

rated from each other. The diameter of the top particle is about 40 nm. The three peaks, namely the RBM ($182\,cm^{-1}$), the G-band ($1590\,cm^{-1}$), and the 2D-band ($2700\,cm^{-1}$) are all nearly equally enhanced in the spectrum obtained with the disconnected grain probe. This result demonstrates again the broad resonance provided by the disconnected grain probe, as predicted by the simulation shown in Figs. 2(c) and (d). The enhancement factor in case of CNT was about 500. We note that this enhancement factor is different than the one observed for graphene (Fig. 4). This is known in literature[46] that the enhancement factor depends on the sample as well as on the Raman mode observed. However, with probes fabricated under the same conditions, the enhancement factor of about 500 was consistently obtained for CNT sample. Figure 5(b) shows a Raman image constructed with the G-band at $1590\,cm^{-1}$, obtained with the disconnected grain probe shown in Fig. 5(a). The sample consisted of two CNT bundles crossing each other, which were dispersed on a glass coverslip. The tip was scanned with a step size of 10 nm in the area of $800 \times 400\,nm^2$. The spatial resolution in this experiment was estimated to be 14 nm, as shown in the inset, which was calculated from the intensity line profile across the CNT bundle (dashed line). Figures 5(c) and 5(d) show the images of the same sample, but represent radial breathing mode (RBM) and 2D-band, respectively. These three images show high signal-to-noise ratio, even though we did not subtract far-field Raman signal as a background. For comparison, the topography of the sample is shown in Fig. 5(e), taken by AFM with a tip-applied force kept at 0.12

nN, which is weak enough to avoid any deformation of the sample or the silver particle on the tip during scanning.

It is known that the silver particles are easily oxidized in air. In our experiments, we also observed enhancement decreases if we use the tip after one or two days. Some researchers have proposed a thin dielectric coating on the tip to protect it from oxidization[47], however, thin spacer layer can reduce the enhancement. In our case, we used the tips immediately after fabrication.

## 3   Conclusions

We have investigated the effect of multiple metal grains on the enhancement of TERS signal. Our principal conclusion is that a group of grains acts as an effective plasmonic antenna to receive and transmit light in nanoscale. Even a single particle works, but multiple grains are more efficient. The value of enhancement changes with the number of grains—there is an optimal number for the grains. Furthermore, spectral broadening has been observed for grains that are closely gathered but separated. The nano-gap between grains is responsible for this spectral broadening. Using a standard vacuum vapor deposition, the grains were successfully structured with a separation length of a few nanometers on a $SiO_2$ cone probe. Using the fabricated probe, we obtained TERS spectral images of CNT bundles with a spatial resolution of 14 nm. The distribution of CNTs was clearly pictured at multiple Raman bands of RBM, G- and 2D-bands. We have estimated the factor of enhancement as 5,500. A higher enhancement is anticipated using a probe with uniformly-sized grains with identical antenna resonances. This can be accomplished for example by attaching mono-dispersed silver nanoparticles on the surface of $SiO_2$ cone using surface modification techniques. Also, fabrication of the probe with an optimal number of grains would be the next technical challenge. The multiple-grain tip structure studied here holds a substantial promise as an efficient TERS probe for molecular imaging and analysis in nanoscale.

## 4   Experimental

**FDTD simulations**

The calculation was performed in three dimensions using finite-difference time-domain (FDTD) method. The mesh size was set at $0.5 \times 0.5 \times 0.5\,nm^3$ inside a rectangular parallelepiped region of $300 \times 300 \times 350\,nm^3$ including the tip, but outside this region, the mesh size gradually became coarser in order to save on computation complexity. The total volume for simulation was $2.2 \times 2.2 \times 2.2\,\mu m^3$. The dielectric constants of Ag and $SiO_2$ were obtained from the literature[48].

**Tip fabrication**

Si cantilever probe for atomic force microscope (AFM) was first thermally oxidized to change the body material from Si to $SiO_2$ [15]. Subsequently, Ag (99.999% purity) was vacuum deposited on the $SiO_2$ cone under a pressure of $\sim 1 \times 10^{-5}\,Pa$. The higher surface free energy of Ag compared with that of $SiO_2$ makes Ag atoms impinging on the surface of $SiO_2$ aggregate to form clusters[49]. The clusters grow in size as the deposition proceeds to form grains. To make disconnected grains, we heated the $SiO_2$ cone up to a temperature of about 600 K during the deposition. On the surface of

high temperature, the deposited atoms diffuse with a higher mobility. This makes the distance between the clusters larger compared with the case without heating, which prevents grains from connecting with each others. We also applied a relatively slower deposition rate of 0.2 Å/s to allow Ag atoms move around freely on the SiO$_2$ surface. We stopped the deposition before grains become connected by occupying the substrate surface (mass thickness of about 40 nm). It was crucial to mount the probe perpendicular to the evaporation source for obtaining uniformly distributed particles with uniform size. For making the connected grains, the deposition was done without heating. Smooth tips were fabricated using higher deposition rate of 1.0 Å/s.

**Sample preparation and experiment procedure** Graphene samples were prepared by mechanical exfoliation of a highly oriented pyrolytic graphite (MikroMasch)[50]. For the preparation of CNT samples, a drop of 1,2-dichloroethane solution of CNT (Meijio Nano Carbon) was spin-casted and dried. The tip was brought into contact with the sample using an AFM head mounted on an inverted optical microscope. The laser, with a wavelength of 488 nm, was passed through a radial polarization converter and focused on the tip apex through an oil-immersion objective lens having an N.A. of 1.4. The Raman scattered signal was collected through the same objective lens and delivered to a Raman spectrometer equipped with a thermoelectrically-cooled CCD camera. The laser power was typically 0.8 mW on the sample. As the probe raster-scanned over the sample with 10 nm step, Raman spectra were recorded pixel-by-pixel with an acquisition period of 300 ms. We evaluated TERS enhancement factors following the formula described in the literatures[9,16].

# References

1   J. Wessel, *J. Opt. Soc. Am. B*, 1985, **2**, 1538–1541.

2   Y. Inouye and S. Kawata, *Opt. Lett.*, 1994, **19**, 159.

3   H. Furukawa and S. Kawata, *Opt. Commun.*, 1998, **148**, 221–224.

4   E. J. Sánchez, L. Novotny and X. S. Xie, *Phys. Rev. Lett.*, 1999, **82**, 4014–4017.

5   N. Hayazawa, Y. Inouye, Z. Sekkat and S. Kawata, *Opt. Commun.*, 2000, **183**, 333–336.

6   R. M. Stöckle, Y. D. Suh, V. Deckert, R. Zenobi and R. Zenobi, *Chem. Phys. Lett.*, 2000, **318**, 131–136.

7   B. Pettinger, G. Picardi, R. Schuster and G. Ertl, *Electrochemistry*, 2000, **68**, 942–949.

8   N. Hayazawa, T. Yano, H. Watanabe, Y. Inouye and S. Kawata, *Chem. Phys. Lett.*, 2003, **376**, 174–180.

9   N. Hayazawa, Y. Inouye, Z. Sekkat and S. Kawata, *J. Chem. Phys.*, 2002, **117**, 1296–1301.

10  A. Hartschuh, E. J. Sánchez, X. S. Xie and L. Novotny, *Phys. Rev. Lett.*, 2003, **90**, 095503.

11  T. Yano, P. Verma, S. Kawata and Y. Inouye, *Appl. Phys. Lett.*, 2006, **88**, 093125.

12  B. Pettinger, G. Picardi, R. Schuster and G. Ertl, *Single Mol.*, 2002, **5**, 285–294.

13  E. Bailo and V. Deckert, *Angew. Chem. Int. Ed.*, 2008, **47**, 1658–1661.

14  X. Cui, W. Zhang, B. S. Yeo, R. Zenobi, C. Hafner and D. Erni, *Opt. Express*, 2007, **15**, 8309–8316.

15  A. Taguchi, N. Hayazawa, Y. Saito, H. Ishitobi, A. Tarun and S. Kawata, *Opt. Express*, 2009, **17**, 6509–6518.

16  B. S. Yeo, W. Zhang, C. Vannier and R. Zenobi, *Appl. Spectrosc.*, 2006, **60**, 1142–1147.

17  S. Maier, P. Kik and H. Atwater, *Appl. Phys. Lett.*, 2002, **81**, 1714–1716.

18  M. L. Brongersma, J. W. Hartman and H. A. Atwater, *Phys. Rev. B*, 2000, **62**, 16356–16359.

19  S. Kawata, A. Ono and P. Verma, *Nat. Photonics*, 2008, **2**, 438–442.

20  J. A. Fan, C. Wu, K. Bao, J. Bao, R. Bardhan, N. J. Halas, V. N. Manoharan, P. Nordlander, G. Shvets and F. Capasso, *Science*, 2010, **328**, 1135–1138.

21  K. R. Li, M. I. Stockman and D. J. Bergman, *Phys. Rev. Lett.*, 2003, **91**, 227402.

22  C. Hoppener, Z. J. Lapin, P. Bharadwaj and L. Novotny, *Phys. Rev. Lett.*, 2012, **109**, 017402.

23  N. Hayazawa, Y. Saito and S. Kawata, *Appl. Phys. Lett.*, 2004, **85**, 6239.

24  J. Takahara, S. Yamagishi, H. Taki, A. Morimoto and T. Kobayashi, *Opt. Lett.*, 1997, **22**, 475–477.

25  R. M. Dickson and L. A. Lyon, *J. Phys. Chem. B*, 2000, **104**, 6095–6098.

26  H. Ditlbacher, A. Hohenau, D. Wagner, U. Kreibig, M. Rogers, F. Hofer, F. R. Aussenegg and J. R. Krenn, *Phys. Rev. Lett.*, 2005, **95**, 257403–257403.

27  T. W. Johnson, Z. J. Lapin, R. Beams, N. C. Lindquist, S. G. Rodrigo, L. Novotny and S.-H. Oh, *ACS Nano*, 2012, **6**, 9168–9174.

28  D. W. Pohl, *Thin Solid Films*, 1995, **264**, 250–254.

29  L. Novotny and N. F. van Hulst, *Nat. Photonics*, 2011, **5**, 83–90.

30  S. Kawata, *Jpn. J. Appl. Phys.*, 2013, **52**, 010001.

31  I. I. Smolyaninov, C. C. Davis, J. Elliott and A. V. Zayats, *Opt. Lett.*, 2005, **30**, 382–384.

32  U. C. Fischer and D. W. Pohl, *Phys. Rev. Lett.*, 1989, **62**, 458–461.

33  T. Sugiura, T. Okada, Y. Inouye, O. Nakamura and S. Kawata, *Opt. Lett.*, 1997, **22**, 1663–1665.

34  T. Okamoto and I. Yamaguchi, *Jpn. J. Appl. Phys.*, 1997, **36**, L166–L169.

35  T. Kalkbrenner, M. Ramstein, J. Mlynek and V. Sandoghdar, *J. Microsc.*, 2001, **202**, 72–76.

36  I. Barsegova, A. Lewis, A. Khatchatouriants, A. Manevitch, A. Ignatov, N. Axelrod and C. Sukenik, *Appl. Phys. Lett.*, 2002, **81**, 3461–3463.

37  T. Umakoshi, T. Yano, Y. Saito and P. Verma, *Appl. Phys. Express*, 2012, **5**, 052001.

38  J. Ando, K. Fujita, N. I. Smith and S. Kawata, *Nano Lett.*, 2011, **11**, 5344–5348.

39  I. Maouli, A. Taguchi, Y. Saito, S. Kawata and P. Verma, *Appl. Phys. Express*, 2015, **8**, 032401.

40  M. Futamata, Y. Maruyama and M. Ishikawa, *J. Phys. Chem. B*, 2003, **107**, 7607–7617.

41  C. Oubre and P. Nordlander, *J. Phys. Chem. B*, 2005, **109**, 10042–10051.

42  M. Futamata, Y. Maruyama and M. Ishikawa, *J. Mol. Struct.*, 2005, **735-736**, 75–84.

43  D.-K. Lim, K.-S. Jeon, H. M. Kim, J.-M. Nam and Y. D. Suh, *Nat. Mater.*, 2010, **9**, 60–67.

44  J.-H. Lee, J.-M. Nam, K.-S. Jeon, D.-K. Lim, H. Kim, S. Kwon, H. Lee and Y. D. Suh, *ACS Nano*, 2012, **6**, 9574–9584.

45  N. Kumar, A. Rae and D. Roy, *Appl. Phys. Lett.*, 2014, **104**, 123106.

46  N. Hayazawa, Y. Inouye, Z. Sekkat and S. Kawata, *Chem. Phys. Lett.*, 2001, **335**, 369–374.

47  C. A. Barrios, A. V. Malkovskiy, A. M. Kisliuk, A. P. Sokolov and M. D. Foster, *J. Phys. Chem. C*, 2009, **113**, 8158–8161.

48  E. D Palik, *Handbook of Optical Constants of Solids*, Academic press, San Diego, 1997.

49  L. I. Maissel and R. Glang, *Handbook of Thin Film Technology*, McGraw-Hill, 1970.

50  K. S. Novoselov, A. K. Geim, S. V. Morozov, D. Jiang, Y. Zhang, S. V. Dubonos, I. V. Grigorieva and A. A. Firsov, *Science*, 2004, **306**, 666–669.

**Nanoscale Accepted Manuscript**